Article

Improvement of MBBR performance by the addition of 3D-printed biocarriers fabricated with 13X and bentonite

Dimitra C. Banti [1,2,*], Petros Samaras [2], Afroditi G. Chioti [1], Anastasios Mitsopoulos [1], Michail Tsangas [3], Antonis Zorpas [3] and Themistoklis Sfetsas [1]

[1] QLAB Private Company, Research & Development, Quality Control and Testing Services, 57008 Thessaloniki, Greece; chioti.a@q-lab.gr; tmitsop@ergoplanning.gr; tsfetsas@q-lab.gr

[2] Department of Food Science and Technology, School of Geotechnical Sciences, International Hellenic University, GR-57400 Thessaloniki, Greece; samaras@ihu.gr

[3] Laboratory of Chemical Engineering and Engineering Sustainability, Faculty of Pure and Applied Sciences, Environmental Conservation and Management, Open University of Cyprus, Latsia P.O. Box 12794, 2252 Nicosia, Cyprus; tsangasm@cytanet.com.cy; antonis.zorpas@ouc.ac.cy

* Correspondence: bantidim@gmail.com (D.B.); Tel.: +30-2310013903

Abstract: In the present work, a comparative evaluation of an MBBR unit performance was carried out for the following cases: when adding 3D-printed biocarriers fabricated with 13X and bentonite, when using K1 commercial biocarriers and when not adding biocarriers at all. For the evaluation of the MBBR efficiency, various physicochemical parameters were measured, while static light scattering and optical microscopy observations were additionally used. Finally, biofilm extracted from the biocarriers was evaluated. The findings suggest that there is an optimal biodegradation of the organic load in all MBBR units. The nitrification and denitrification process were improved at the 3D MBBR as compared to the control MBBR and MBBR K1. The dry mass of the biofilm in the 3D-printed biocarriers was two orders of magnitude larger than the one in the K1 biocarriers. What is more, in the K1 biocarriers the mass of the biofilm varied in relation to time, due to the fact that it could not be kept inside the holes, something that was not observed to happen with the 3D-printed biocarriers. Finally, it was observed, mostly in the 3D MBBR and less in the K1 MBBR, that the growth of nitrifying bacteria and heterotrophs inside the units increased the biomass production in the form of SMP, which in turn favored the adhesion of biomass on the surface of biocarriers.

Keywords: moving bed biofilm reactor; K1 biocarriers; 3D-printed biocarriers; biofilm; SMP; EPS; activated sludge; wastewater treatment

1. Introduction

Moving bed biofilm reactors (MBBR) are widely used for applying biocarriers during aerobic wastewater treatment [1]. There are more than 1,200 large-scale MBBR units with a capacity of 200 population equivalents (p.e.) or more, and 7,000 units with a capacity of less than 200 p.e. operating worldwide and processing either urban wastewater or industrial wastewater [1]. MBBR technology is an advanced technology with low cost of capital, low operating, maintenance and replacement costs while at the same time it is also simple, reliable and stable to use, and allows all processes to take place in one tank [2,3]. Compared to other wastewater treatment methods, MBBR is a financially and environmentally competitive method, as it does not require the constant addition of costly reagents and it does not produce dangerous residuals [1,4,5].

MBBRs use freely moving submerged biocarriers in aeration tanks combining two different processes; the processes of attached and suspended biomass growth. All the biological processes that take place are mainly due to the biomass formed in the biocarriers [6]. Therefore, each biocarrier increases the performance of the unit by providing a protected surface for the growth of autotrophic

 doi:10.20944/preprints202306.0207.v1

and heterotrophic microorganisms in wastewater and, thus, achieving high rates of degradation. In systems like these, biomass can be grown both in suspended biocarriers and in steadily placed biofilters, resulting in an increase of the biomass in the reactor and achieving a better effluent quality [7]. For the biofilm reactors to function properly, a steady-state biofilm should be formed on the surface of the biocarriers [8].

Sequencing batch reactors (SBR) are activated sludge processing units, in which all stages of wastewater processing are performed consecutively in the same reactor [9]. These reactors are processing systems which are especially flexible, inexpensive to built and particularly efficient. In these reactors, the time needed for aerobic and anoxic processes in an operating cycle can be alternated, something that provides flexibility during the removal of organic load, nitrogen and phosphorus, and at the same time the possibility for variation in the time needed for the different phases of the process, thus, maximizing the performance of each phase [10]. The SBRs' performance greatly increases when they are combined with the addition of biocarriers.

A critical parameter that determines the performance of MBBR technology is the appropriate design of the biocarrier [11]. Some of the optimal biocarriers characteristics that significantly affect the MBBR performance are the large specific surface area per unit of volume, the material they are made of, their surface characteristics, their orientation, the distance among the pores and their geometry [12,13]. 3D printing technology can contribute to the design of the optimal biocarrier by offering flexibility in its design and in the selection of its manufacturing material. A lot of research has been conducted to date, attempting to analyze and improve this advanced wastewater treatment method. Tang et al. (2017) [8] have found out that, in moving bed bioreactors with biocarriers, COD removal reached a high percentage (> 80%) after a very short period of time, fluctuating during the first 10 days, and then it increased reaching a percentage which exceeded 90%. On the contrary, Elliot et al. (2017) [13] discovered a maximum removal of COD and NH_4-N which reached 77% and 34% respectively in the first 5 days. They also observed that the amount of ammonia and nitrates was reduced over time, suggesting that processes of nitrification were taking place. Proano-Pena et al. (2020) [14] have studied various kinds of biocarriers that were manufactured using 3D printing while gradually increasing the specific surface area of the biocarriers for their studies. After comparing three biocarriers which did not have the same specific surface area, it was concluded that the optimal specific surface area for aerobic wastewater treatment was 1,168 m^2/m^3. Dong et al. (2015) [7] created a series of three-dimensional hollow honeycomb spherically-structured biocarriers, formed from pentahedrons and hexahedrons for the removal of COD and NH_3. These biocarriers activated an alternative method of mass transfer from the biocarriers towards the biofilm. Elliot et al. (2017) [13] created spherical biocarriers with a larger specific surface area, something that increased the NH_3 removal rate by 1,620 ppm/d compared to common biocarriers. It is worth mentioning that the research of Chioti et al (2022) [15], who studied the efficiency of Kaldnes K1 commercial biocarriers and 3D-printed biocarriers with 13X and bentonite in aerobic wastewater treatment performed in lab reactors of 150 mL active volume, has also shown a remarkable efficiency in wastewater treatment. According to other researchers [16], the synthetic biofilm carriers showed unstable COD removal rates, in contrast to the natural biofilm carriers that did not present any instability. This is due to the surface properties of the natural biofilm carriers, such as surface pores and roughness. According to Alamshawee et al. (2022) [16], the Kaldnes K1 biocarriers delivered the shortest start-up in the first 3 days.

Some of the main characteristics of the activated sludge that play an important role in each wastewater treatment process are the soluble microbial products (SMP) and the extracellular polymeric substances (EPS) [17]. SMPs and EPSs determine the physicochemical and biological characteristics of the activated sludge and constitute a basic component of its structure. More specifically, they comprise a gel-like biofilm matrix that is particularly hydrated and often loaded, in which microorganisms are integrated and immobilized. The percentage of EPS in the biofilm ranges from 50 to 90% of the total organic matter [18]. Bassin et al. [19] have suggested that the organic matter at the initial stage enables the growth of nitrifying bacteria and heterotrophs. On the other hand, the growth of nitrifying bacteria and heterotrophs increases biomass production; thus, SMP and EPS generation is

Preprints (www.preprints.org) | NOT PEER-REVIEWED | Posted: 2 June 2023 doi:10.20944/preprints202306.0207.v1

increased. The high production of SMP and EPS favors the adhesion of biomass on the surface of biocarriers [20].

The aim of this study is the comparative evaluation of the following three cases taking place in an MBBR unit: the addition of 3D printed biocarriers fabricated with 13X and bentonite, the addition of the widely-used Kaldnes K1 commercial biocarriers and the non-addition of biocarriers. In this research paper, the efficiency of wastewater treatment processes in relation to organic load and nitrogen removal will be assessed. Its correlation with the characteristics of the activated sludge, for example the size of aggregates and the SMP/EPS concentration, and the growing biofilm on the surfaces of the biocarriers will be assessed as well.

2. Materials and Methods

2.1 Moving Bed Biofilm Reactor set-up and operating conditions

For the purposes of this research, an MBBR with a total active volume of 2.5 L was used, the flow diagram of which is presented in **Figure 1**. The unit operated as an SBR and each operating cycle included the following phases: feed (30 min.) with a Qin = 1.8 L/h, anoxic phase (30 min), aerobic phase (6 h), sedimentation (30 min) and outflow (30 min) with a Qout = 1.8 L/h. The MBBRs consisted of 1 dissolved oxygen measuring device, 2 peristaltic pumps, an air compressor, a thermometer and a PLC system (Eutech Instruments), which was used for documenting and setting the operation parameters with the help of SCADA software (Simantec, Siemens). The parameters documented and set via SCADA software included the concentration of dissolved oxygen in the tank, the temperature, inflow and outflow, as well as the alternate operation stages of the unit.

The MBBR was powered by synthetic sewage which was prepared twice a week with the following composition: glucose (250 mg/L), corn starch (250 mg/L), NH_4Cl (100 mg/L), peptone (28 mg/L), KH_2PO_4 (26.5 mg/L), $MgSO_4 \cdot 7H_2O$ (9 mg/L), $MnSO_4 \cdot H_2O$ (3.7 mg/L), $FeSO_4 \cdot 7H_2O$ (0.55 mg/L) and $NaHCO_3$ (120 mg/L) [21,22]. At the start of the experiment, activated sludge from a wastewater treatment plant in Thessaloniki was added to the MBBR tank for the acclimatization of the synthetic sewage.

Three continuous flow experiments were conducted each one lasting more than one month. Since during the first experiment no biocarriers were added to the unit, the first experiment will be hereinafter referred to as **control MBBR**. During the second experiment, commercial Kaldnes K1 biocarriers were added in the unit with a total volume of 1 L (**Figure 2 (a)**). This experiment will be hereinafter referred to as **MBBR K1**. During the third experiment, 3D-printed biocarriers manufactured with 13X and bentonite (**Figure 2 (b)**) with a total volume of 1 L as well were added in the unit. This experiment will be hereinafter referred to as **MBBR 3D**. Before adding the biocarriers in the unit in the second and third experiment, the biocarriers were placed in an aerated laboratory wastewater treatment tank for around two months, in order to facilitate the growth of biofilm on their surface.

Preprints (www.preprints.org) | NOT PEER-REVIEWED | Posted: 2 June 2023 doi:10.20944/preprints202306.0207.v1

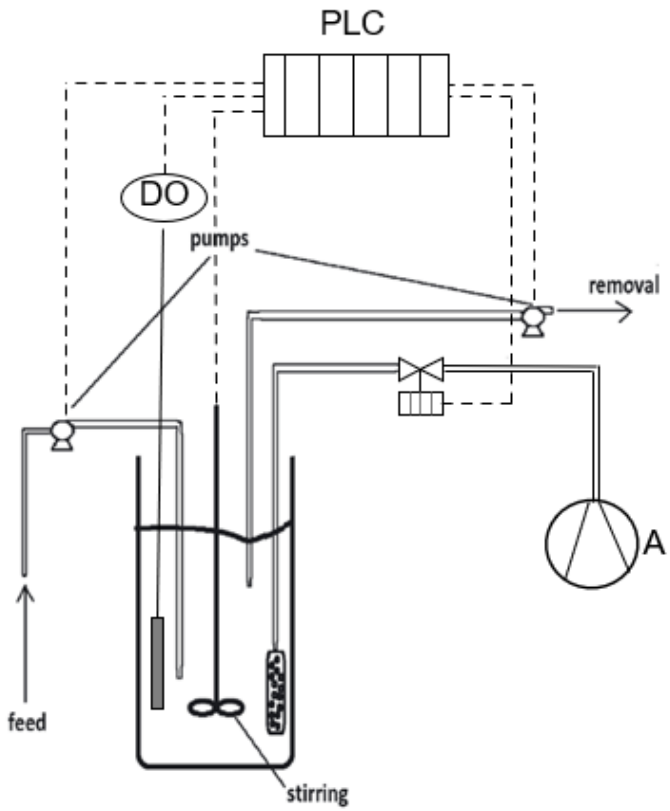

Figure 1. MBBR flow diagram in which A: Air Compressor, DO: Dissolved Oxygen measuring device and PLC: Programmable Logic Controller.

The COD variation in the inflow of all three units was 272±22 mg/L, the MLSS 2.3±0.1 mg/L and the hydraulic retention time (HRT) was 18 h. The value of Food/Microorganisms (F/M) loading equaled 0.08 g COD/g MLSS/d and therefore varied within the desirable value range for the effective wastewater treatment in aerobic units. In all three experiments similar loading was used so that the results could be compared.

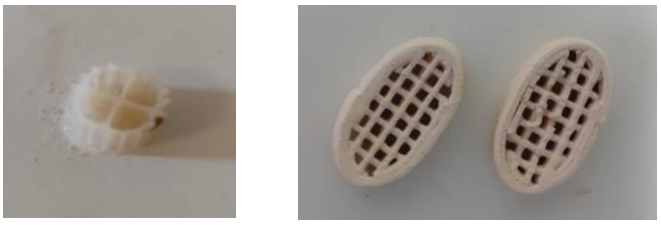

(**a**) (**b**)

Figure 2. (**a**) Commercial Kaldnes K1 biocarriers and (**b**) 3D-printed biocarriers manufactured with 13X and bentonite.

2.2 Biofilm extraction method

Biocarrier samples were regularly taken from the MBBRs and the biofilm that was grown on their surface was extracted in order to determine its dry mass and its SMPs. The extraction of biofilm was carried out in the following way: the biocarrier sample was placed in deionized water of 10 mL volume, stirred in a vortex device for 1 minute, then placed in an ultrasonic device for 2 minutes, and finally stirred again in a vortex device for one more minute, using the method of Mandakhalikar et al. (2018) [23,24]. This methodology played a role in the complete removal of the biofilm.

Preprints (www.preprints.org) | NOT PEER-REVIEWED | Posted: 2 June 2023 doi:10.20944/preprints202306.0207.v1

2.3 Printing methodology of the 3D-printed biocarriers with 13X and bentonite

For the preparation of the printing paste, the ceramic material (13X), the inorganic (bentonite) and the organic binders were mixed in a mortar until this mixture of solids was homogenized. Then, the deionized water was mixed with colloidal silica. Finally, the aqueous mixture of water and colloidal silica was gradually added to the above-mentioned mixture of solids, while at the same time the mixture was being fused with a pestle until the paste was homogenized. A 45μm-hole-diameter sieve was also used to remove all aggregates and grains from the paste. **Table 1** below shows the zeolite and inorganic binders proportions.

Table 1. Zeolite and clay proportion.

	Material	Paste content	Zeolite/clay percentage
Zeolite	13X	45%	89%
Inorganic binder	Bentonite	6%	11%
Colloidal silica	Ludox AS-40	14%	
	Water	34%	
Organic binder	Methyl cellulose	1%	

The material was then centrifuged to remove any air bubbles, transferred to the syringe and finally to the printer. The next process that took place was the preparation of the printer. This process included the creation of 3D geometry, during which parameters like the shape of the biocarrier, the recurring geometric pattern, the height of each layer, the nozzle diameter, the pressure and the printing speed were determined. The recurring geometric pattern chosen for the biocarriers was rectilinear and the dimensions of the biocarrier were: 24 mm width, 14 mm length, 7 mm height and 1.1264 g weight. The printing was performed using the BIO X6 (Cellink) printer.

2.4 Determination of the physicochemical parameters

The physicochemical parameters for the characterization of the influent and effluent wastewater as well as of the wastewater during the anoxic and aerobic phase (COD, Total N, NH_4-N, NO_3-N and PO_4-P) were determined using the Hack–Lange LCK kits, along with a DR-2800 spectrophotometer. The soluble fraction of the activated sludge that was produced after filtration on a filtration device was measured in a filter with 1.2-μmc-sized pores during the anoxic and aerobic phases. Mixed liquor suspended solids (MLSS) were measured according to standard methods [25]. The measurements were performed regularly to evaluate the progress of the experiments and the performance of MBBR treatment.

Dissolved oxygen (DO) was measured, documented and set on a constant basis. The measurement was performed using a Greisinger OXY 3610 MP measuring electrode.

Samples were taken on a regular basis during the anoxic and aerobic phases to measure SMP and EPS. For SMP and EPS extraction, a natural thermal extraction method was used [26,27]. To measure the extracted SMP and EPS protein content, the modified Lowry method was repeated three times [28], while to measure the SMP and EPS carbohydrate content the photometric method proposed by Dubois et al. (1956) [29] was repeated two times. Bovine Serum Albumin (BSA, Sigma Aldrich) was used for the preparation of the protein calibration curve while glucose (Panreac) was used for the preparation of the carbohydrates calibration curve.

Static light scattering (Mastersizer, Malvern) was used to determine the size distribution of aggregates with a diameter larger than 10 μm in mixed liquor. Activated sludge was also viewed under a Light Sheet Microscope (LSM, Observer Z1, Zeiss, Oberkochen, Germany) and filamentous index (FI) evaluation was also performed [30,31], during which the population of filamentous microorganisms in the activated sludge mixed liquor was measured. The microscope images were edited using ZEN software.

 doi:10.20944/preprints202306.0207.v1

2.5 DNA extraction and 16S rRNA gene amplicon sequencing

The biofilm suspensions were subjected to genomic DNA extraction using the DNeasy PowerSoil Pro Kit (QIAGEN, Hilde, Germany), following the manufacturer's protocol. The 16S Metagenomic Sequencing Library Preparation protocol (IlluminaTM, Inc., San Diego, CA, United States) was used to prepare the library according to standard guidelines. Briefly, the 341f/805r primer pair, which targets the bacterial and archaeal V3–V4 hypervariable regions of the 16S rRNA gene (341f 5′-CCTACGGGNGGCWGCAG-3′, 805r 5′-GACTACHVGGTATCTAATCC-3′), was used to amplify the DNA. The produced DNA libraries were quantified with the Qubit™ 4 Fluorometer (Thermo Fisher Scientific, Waltham, MA, USA), and their size was verified by 1.5 % agarose gel electrophoresis. Equimolar concentrations of the libraries were pooled, and a quantitative PCR was performed with the QIAseq Library Quant Assay Kit (QIAGEN, Germany) to evaluate the library concentration. The pooled library was spiked with 25% phiX control library (Illumina Inc., San Diego, CA, USA), denatured, and diluted to a final concentration of 6 pM. Sequencing was performed on an Illumina MiSeqTM platform using the MiSeq Reagent Nano Kit version 2 (500-Cycle)/ MiSeq Reagent Kit version 3 (600-Cycle) chemistry for a paired-end, 2x250-bp/2x300 cycle run.

2.2. Bioinformatics

The analysis of the data obtained from the sequencing was carried out using Quantitative Insights Into Microbial Ecology 2 (QIIME2) software, version 2022.2 [32]. The Amplicon Sequence Variants (ASVs) were generated using the DADA2 algorithm [33], which involved quality-based trimming, filtering, and chimera detection and removal. The taxonomic annotation of the reads was carried out using the SILVA reference database (SSU, release 138) [34]. The phylogenetic diversity was measured using Faith's Phylogenetic Diversity and weighted and unweighted UniFrac metrics. The q2-diversity plugin was used to compute several metrics for alpha and beta diversity analysis, and the resulting data were used to generate principal coordinates analysis (PCoA) plots using Emperor for each beta diversity.

3. Results

3.1 Wastewater treatment efficiency and physicochemical parameters at the 3 MBBRs

In this chapter, the results of the 3 MBBR experiments are compared and presented. DO during the aerobic phase was controlled at 2.0-4.0 mg/L for an efficient wastewater biodegradation [35] but also for having similar conditions in all three experiments. More specifically in control MBBR, DO ranged from 3.1±0.7 mg/L, in MBBR K1 from 2.6±0.8 mg/L and in MBBR 3D from 2.8±0.6 mg/L.

Figure 3 shows the COD concentration diagrams comparatively for the influent and effluent in all three experiments, as well as the soluble COD concentration for the anoxic and aerobic phases.

Preprints (www.preprints.org) | NOT PEER-REVIEWED | Posted: 2 June 2023 doi:10.20944/preprints202306.0207.v1

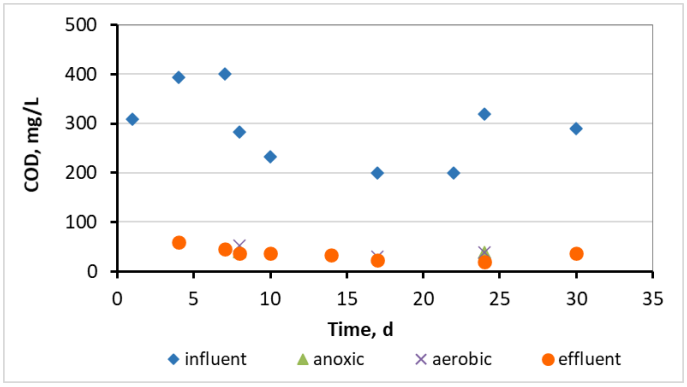

(a)

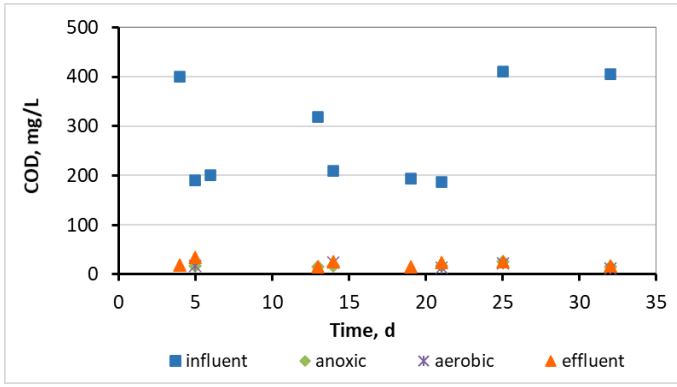

(b)

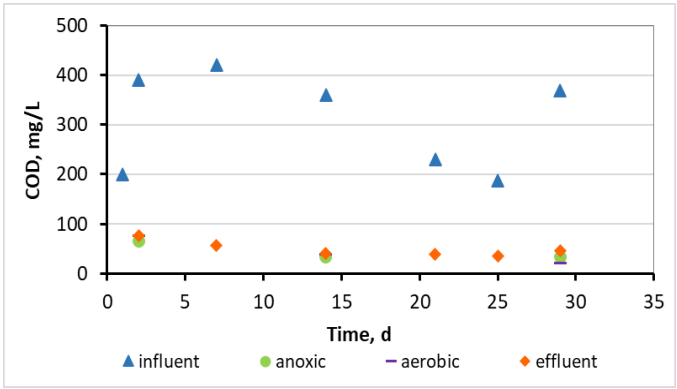

(c)

Figure 3. COD concentration diagrams for (a) control MBBR, (b) MBBR K1 and (c) MBBR 3D. .

Figures 4, 5 and **6** show the NO_3-N, NH_4-N and Total N concentration diagrams comparatively for the influent and effluent respectively in all three experiments, as well as the soluble NO_3-N, NH_4-N and Total N concentration for the anoxic and aerobic phases.

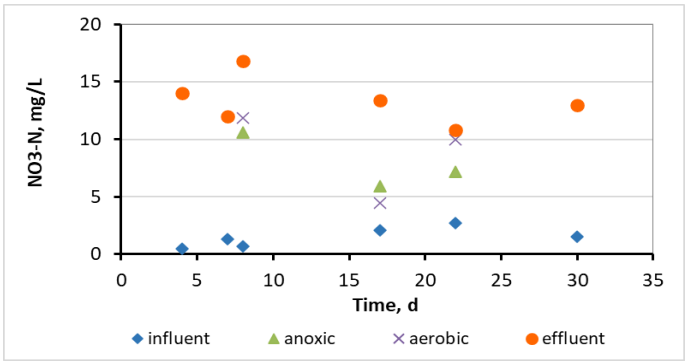

(a)

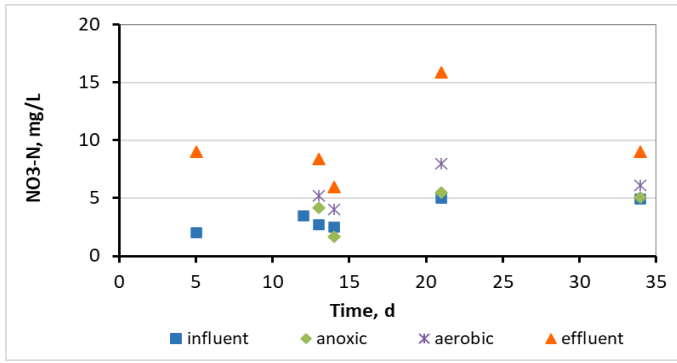

(b)

Preprints (www.preprints.org) | NOT PEER-REVIEWED | Posted: 2 June 2023 doi:10.20944/preprints202306.0207.v1

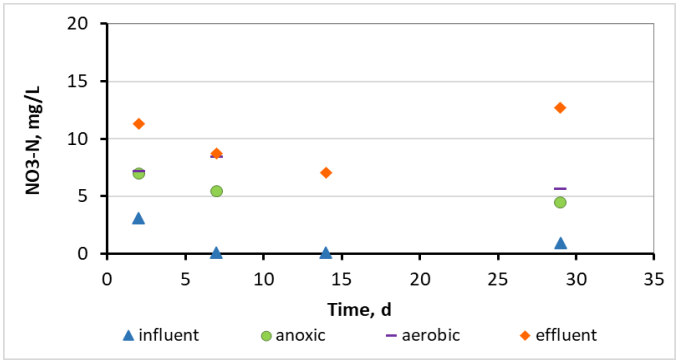

(c)

Figure 4. NO_3-N concentration diagrams for (**a**) control MBBR, (**b**) MBBR K1 and (**c**) MBBR 3D. .

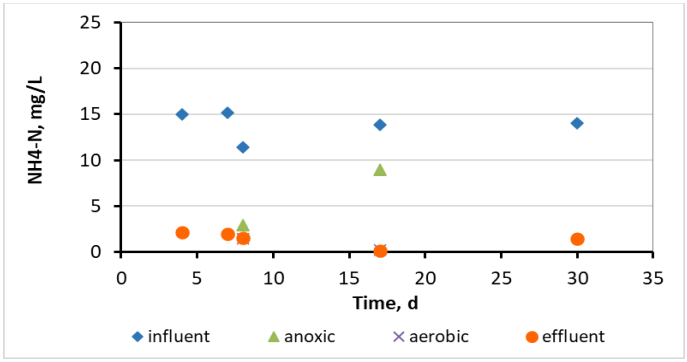

(a)

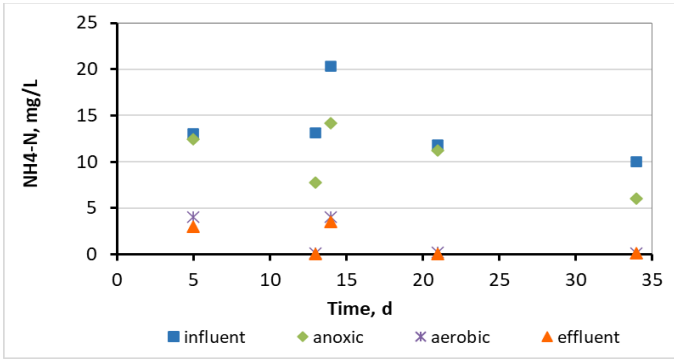

(b)

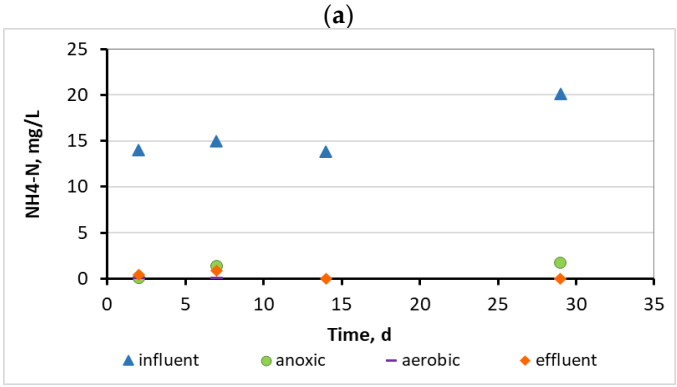

(c)

Figure 5. NH_4-N concentration diagrams for (**a**) control MBBR, (**b**) MBBR K1 and (**c**) MBBR 3D. .

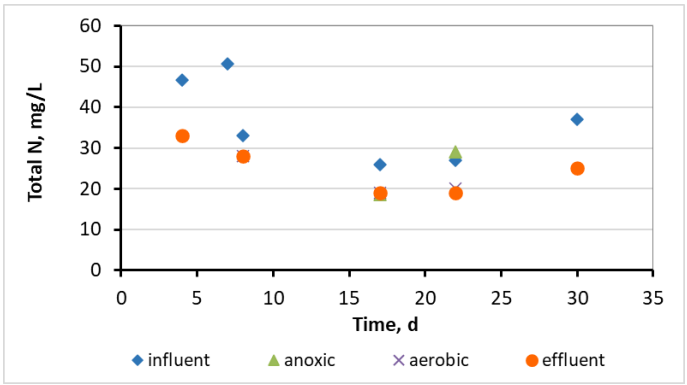

(a)

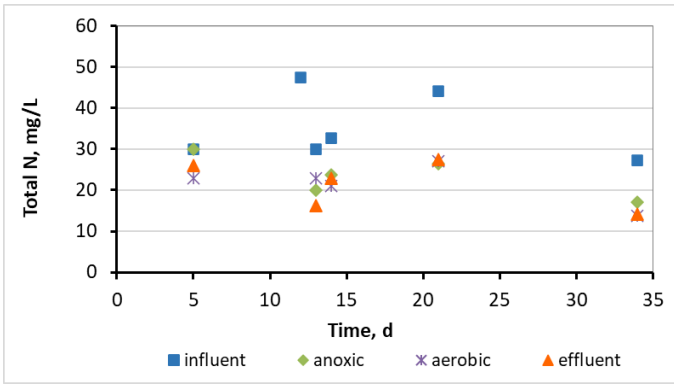

(b)

Preprints (www.preprints.org) | NOT PEER-REVIEWED | Posted: 2 June 2023 doi:10.20944/preprints202306.0207.v1

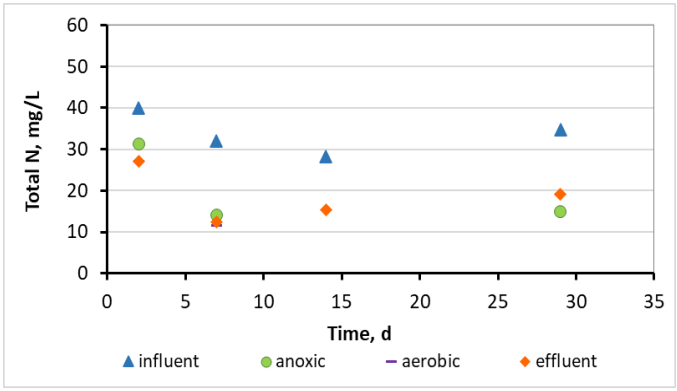

(**c**)

Figure 6. Total N concentration diagrams for (**a**) control MBBR, (**b**) MBBR K1 and (**c**) MBBR 3D. .

Figures 7 and **8** show the SMP proteins and SMP carbohydrates concentration diagrams for the anoxic and aerobic phases of all three MBBR units. The respective diagrams of EPS proteins and EPS carbohydrates concentration for the anoxic and aerobic phases of all three MBBR units are shown in **Figures 9** and **10**.

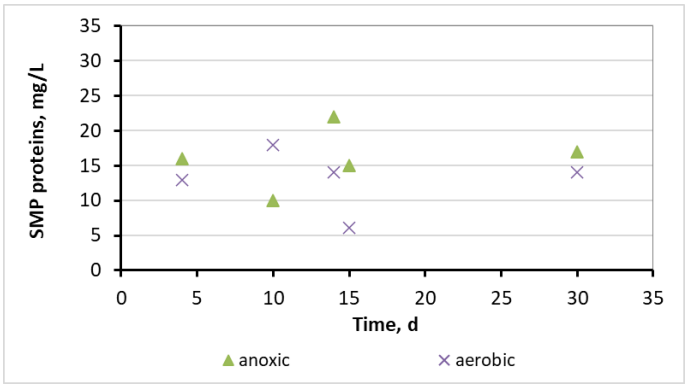

(**a**)

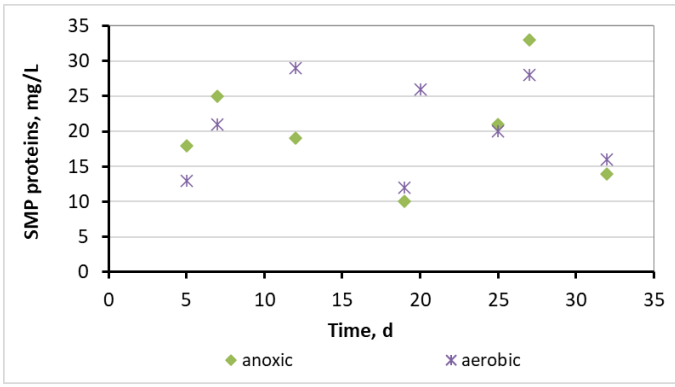

(**b**)

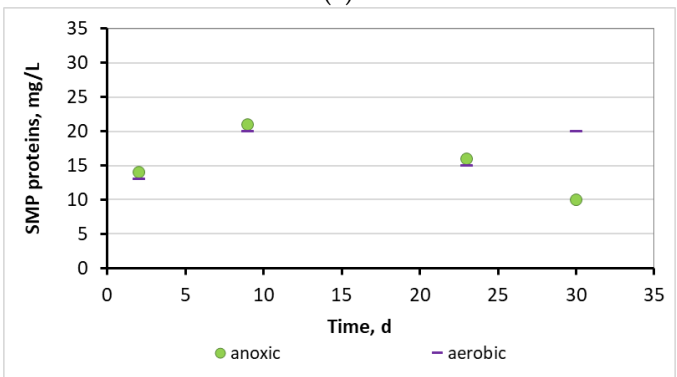

(**c**)

Figure 7. SMP proteins concentration diagrams for anoxic and aerobic phase for (**a**) control MBBR, (**b**) MBBR K1 and (**c**) MBBR 3D. .

Preprints (www.preprints.org) | NOT PEER-REVIEWED | Posted: 2 June 2023 doi:10.20944/preprints202306.0207.v1

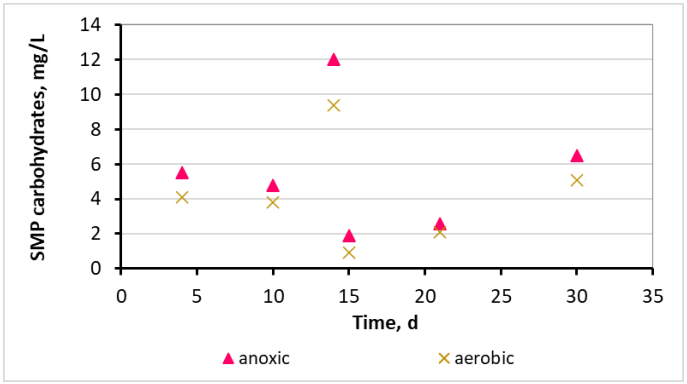

(a)

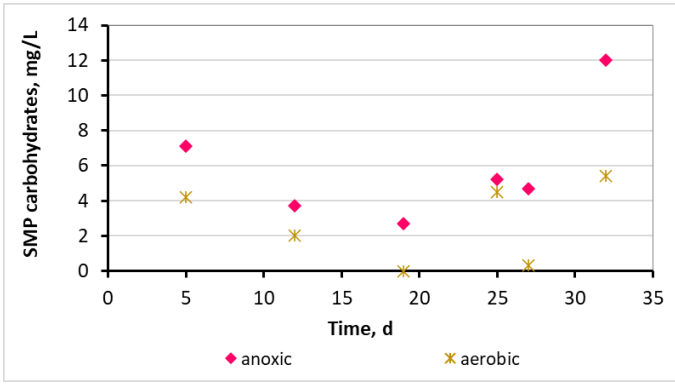

(b)

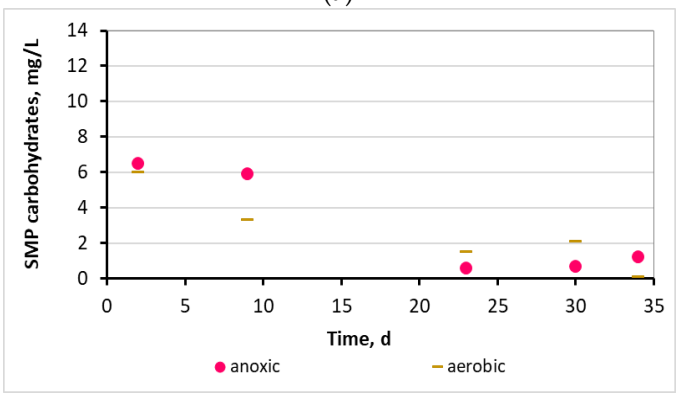

(c)

Figure 8. SMP carbohydrates concentration diagrams for anoxic and aerobic phase for (**a**) control MBBR, (**b**) MBBR K1 and (**c**) MBBR 3D. .

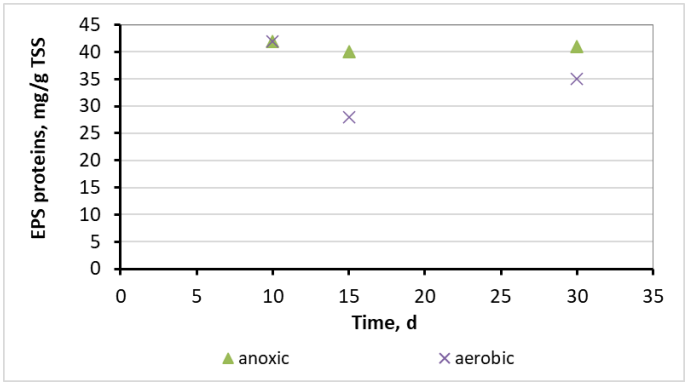

(a)

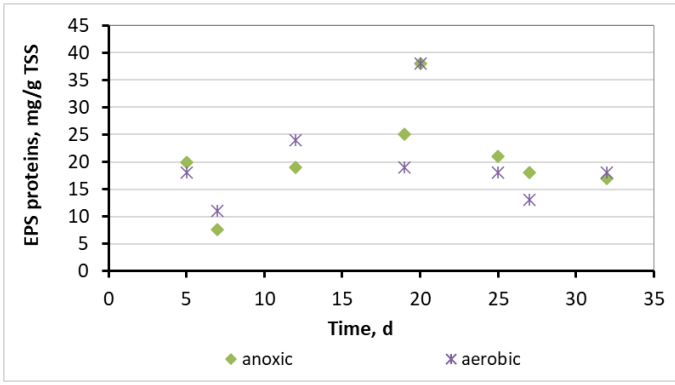

(b)

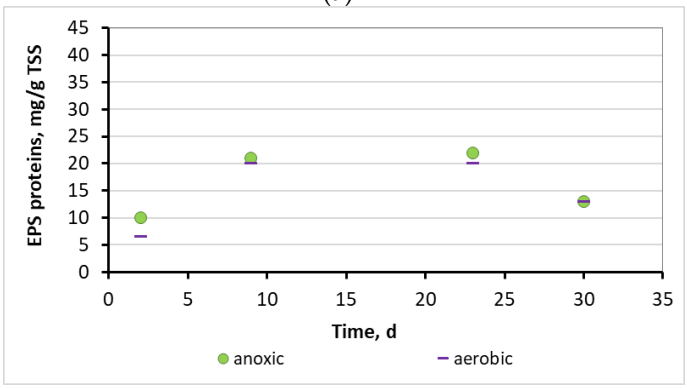

(c)

Figure 9. EPS proteins concentration diagrams for anoxic and aerobic phase for (a) control MBBR, (b) MBBR K1 and (c) MBBR 3D. .

Preprints (www.preprints.org) | NOT PEER-REVIEWED | Posted: 2 June 2023 doi:10.20944/preprints202306.0207.v1

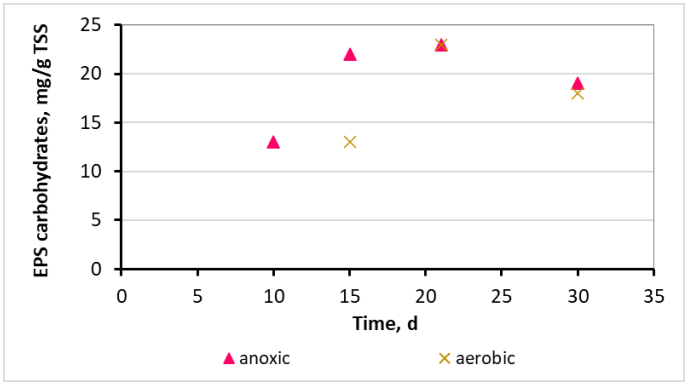

(a)

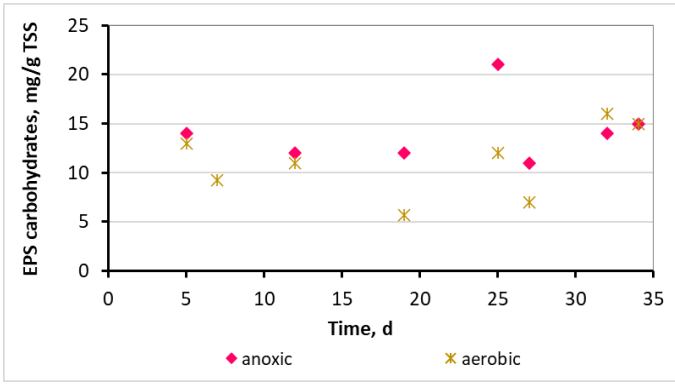

(b)

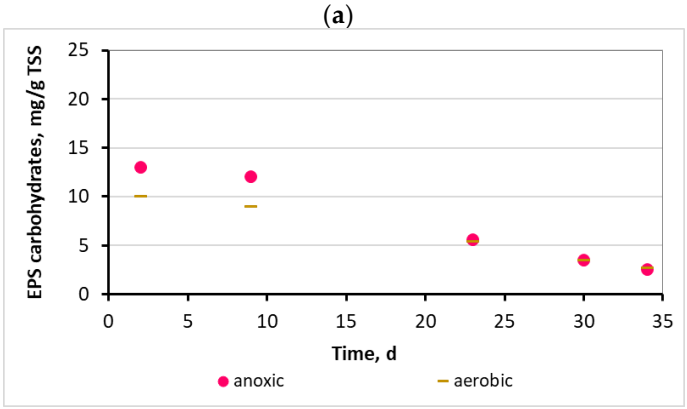

(c)

Figure 10. EPS carbohydrates concentration diagrams for anoxic and aerobic phase for (**a**) control MBBR, (**b**) MBBR K1 and (**c**) MBBR 3D.

Figure 11 depicts a standard image of activated sludge taken from an optical microscope. In the anoxic phase, the aggregates' size for the control MBBR was equal to 82±20 μm, for the MBBR K1 it was 72±13 μm and for the MBBR 3D it was 174±29 μm. The size of the aggregates seemed to increase in relation to the operating time of the units in MBBR K1 and MBBR 3D. This is presented in **Figure 12.**

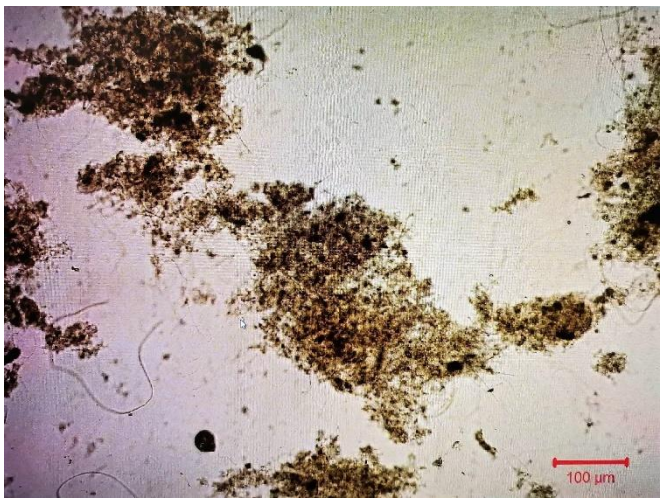

Figure 11. Standard image of the activated sludge mixed liquor during the operation of the units. .

Preprints (www.preprints.org) | NOT PEER-REVIEWED | Posted: 2 June 2023 doi:10.20944/preprints202306.0207.v1

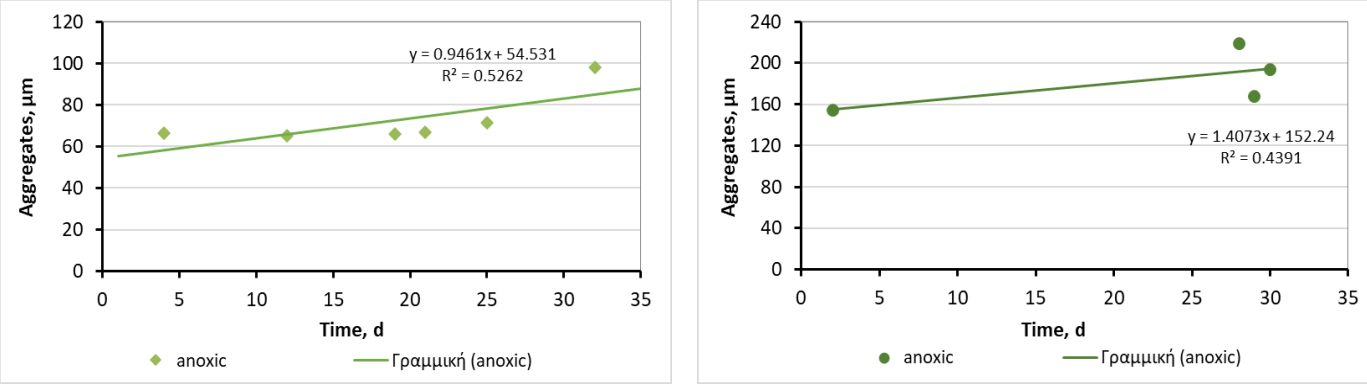

(**a**) (**b**)

Figure 12. Size of the aggregates in the mixed liquor of the anoxic phase (**a**) for the MBBR K1 and (**b**) for the MBBR 3D experiments.

3.2 Evaluation of the biofilm developed on the surfaces of biocarriers

3.2.1 Biofilm developed at the Kaldnes K1 biocarriers

Figure 13 shows the biocarriers and the biofilm that was developed on the inside of their surfaces in relation to time. The dry mass of the biofilm that was developed in the biocarriers in relation to the operating time of the unit is presented in **Table 2.** The measurements regarded the biofilm that was developed on the surface of 5 biocarriers per day of measurement after its extraction. The SMP proteins values in the biofilm of K1 biocarriers ranged from 19±3.5 mg/L and the SMP carbohydrates values from 4.0±0.9 mg/L.

(**a**) (**b**)

Figure 13. Biocarriers with the formed biofilm on the (**a**) 14th day and (**b**) 29th day of unit operation.

Table 2. Dry mass of the biofilm developed in the biocarriers in relation to the operating time of the unit.

t, d	Dry mass of biofilm, mg
14	3.5±0.003
21	3.2±0.007
29	4.5±0.004
35	3.1±0.004

3.2.2 Biofilm at the 3D-printed biocarriers developed with 13X and bentonite

In the following figure, **Figure 14,** the biocarriers and the biofilm that was developed on the inside of their surfaces in relation to time are presented. The dry mass of the biofilm in relation to the operating time of the unit is presented in **Table 3.** The measurements in this case as well regarded the biofilm that was developed on the surfaces of 5 biocarriers after its extraction. The SMP proteins values in the biofilm of 3D-printed biocarriers ranged from 17±3.4 mg/L and the SMP carbohydrates values from 2.8±2.5 mg/L.

Preprints (www.preprints.org) | NOT PEER-REVIEWED | Posted: 2 June 2023 doi:10.20944/preprints202306.0207.v1

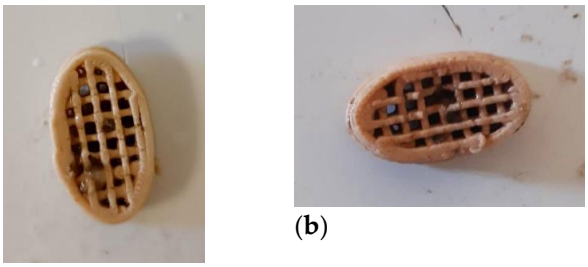

(**a**) (**b**)

Figure 14. Biocarriers with the formed biofilm on the (**a**) 13th day and (**b**) 26th day of unit operation.

Table 3. Dry mass of the biofilm developed in the biocarriers in relation to the operating time of the unit.

t, d	Dry mass of biofilm, mg
7	772±117
13	831±46
21	700±121
26	641±76
35	867±161

3.2.3 Biofilm microbiome analysis on biocarriers through 16S rRNA sequencing

The results concerning the 16S rRNA microbiome analysis of the biofilm formed on the surface of both K1 and 3D-printed biocarriers on day 30 of the experiment showed that the most abundant phyla were *Proteobacteria* (27.7-45.1% of total reads), *Actinobacteria* (8.2-27.4%), *Firmicutes* (13.5-21.9%), and *Bacteroidetes* (1.25-13.1%) (**Figure 15**). The dominant classes for the 3D-printed biocarriers included *Actinobacteria* (27.4%), *Alphaproteobacteria* (18.14%), *Bacilli* (14.9%), and *Clostridia* (6.3%) while in the case of K1 *Alphaproteobacteria* (19.5%) prevailed, followed by *Gammaproteobacteria* (17.8%), *Bacilli* (10.8%) and *Actinobacteria* (8.2%). *Planctomycentia* were also found to a lesser degree with comparable abundances in both biocarriers (5.1% in 3D-printed and 6.1% in K1). At family level, *Bacillales Incertae Sedis family XII* (8.4%), *Planctomycetaceae* (5.1%), *Mycobacteriaceae* (5%), *Caulobacteraceae* (4.9%), *Carnobacteriaceae* (3.7%), *Rhodobacteraceae* (3.5%), and *Solirubrobacteraceae* (3.5%) were highly enriched in 3D-printed biocarriers. Conversely, K1 biocarriers were mostly characterized by *Rhodobacteraceae* (13.5%), *Moraxellaceae* (7.3%), *Planctomycetaceae* (6.2%), *Staphylococcaceae* (4.8%), *Saprospiraceae* (4.7%), *Aeromonadaceae* (3.9%), and *Caldilineaceae* (3.6%). Among the genera detected, the most abundant in the case of the 3D-printed biocarriers were *Exiguobacterium* (8.4%), *Mycobacterium* (4.7%), *Phenylobacterium* (4.5%), *Trichococcus* (3.6%), and *Solirubrobacter* (2.7%), while in K1 biocarriers, *Acinetobacter* (7%) dominated, together with *Gemmobacter* (4.8%), *Staphylococcus* (4.7%), *Paracoccus* (3.4%), *Litorilinea* (2.9%), and *Exiguobacterium* (2.6%). The relative abundances of the microbial groups detected in the biofilm of 3D-printed carriers collected at 25 days of operation were slightly lower than those of 35 days regarding the aforementioned genera, except for *Exiguobacterium* (3.7%) and *Trichococcus* (0.4%), which exhibited quite lower numbers (data not shown). The corresponding sludge from which the 3D-printed biocarriers were collected (day 30) had a comparable microbial composition to the one within the biofilm on the biocarriers. Some families, though, were detected at differing levels, such as *Planctomycetaceae* (8.5%) and *Carnobacteriaceae* (6.4%), which were more enriched, or Caulobacteraceae (2.8%), *Mycobacteriaceae* (2.6%), and *Bacillales Incertae Sedis family XII* (0,4%), which were less abundant. Moreover, at genus level, lower numbers of *Mycobacterium* (2.4%) and *Phenylobacterium* (2.7%) were observed and, interestingly, *Exiguobacterium* were only found at 0.4%. Slightly higher were the levels of *Trichococcus* (6.3%) and *Candidatus saccharibacteria Incertae Sedis* (2.3%), which were detected at 1.7% in the 3D-printed biocarriers. Figures 1 and 2 depict the most highly abundant families and genera, respectively, found within the biofilm of K1 and 3D-printed biocarriers, as well as in the sludge of the latter.

Preprints (www.preprints.org) | NOT PEER-REVIEWED | Posted: 2 June 2023 doi:10.20944/preprints202306.0207.v1

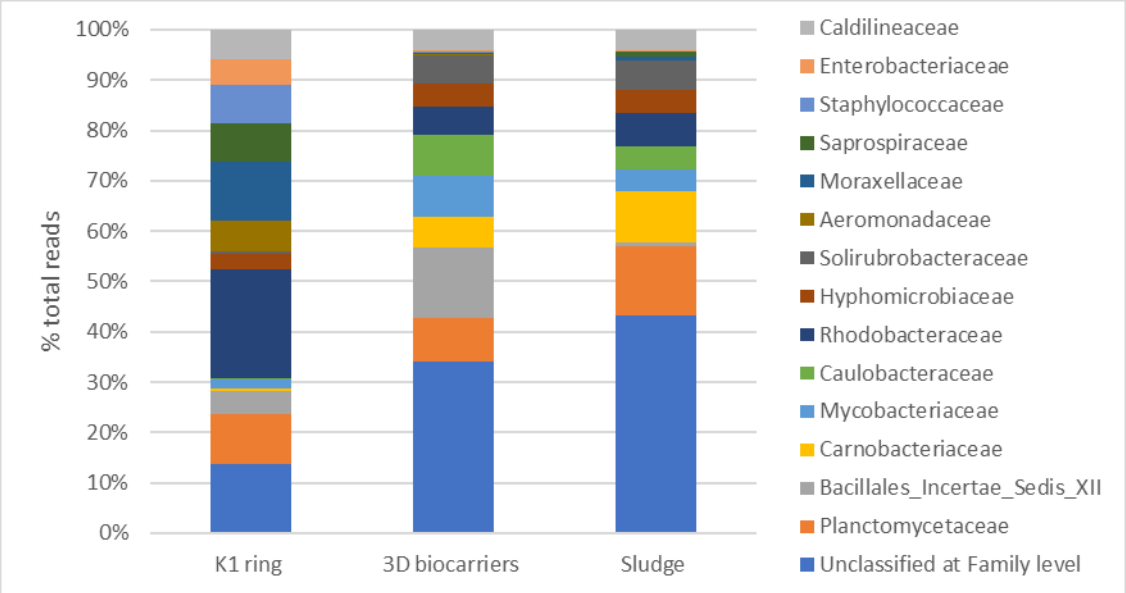

Figure 15. Relative abundance of the major families detected on the biofilm of K1 ring, 3D-printed biocarriers, and sludge at 30 days of operation.

4. Discussion

Based on **Figure 3** and on the influent/affluent COD values, it can be concluded that there is an excellent effluent quality in all three cases, with a removal rate of 88% for the control MBBR, 92% for MBBR K1 (slightly increased) and of 84% for MBBR 3D (slightly decreased). Other researchers [16] have concluded that COD removal when using synthetic biocarriers (including Kaldnes K1 biocarriers) in smaller-scale experiments is unstable. However, this was not found in the large-scale experiments of this research, as the COD removal was increasing steadily during the operating time of the unit. The values of the soluble COD in the anoxic and aerobic phase in all three MBBR units was close to the effluent COD values, meaning that removal of the organic load of wastewater was already taking place since the anoxic phase. The excellent effluent quality can be determined by comparing it to the COD limit values acceptable for wastewater discharge in water bodies. According to the World Bank Group, for the effluent quality to be characterized as excellent, either the COD value should be 125 mg/L or the minimum COD removal rate during wastewater treatment should be 75% [36].

The value of NO_3-N in control MBBR increased by 89% (**Figure 4**) in the influent of the unit, while during the anoxic and aerobic phase intermediate values were observed between the influent and the affluent values. The value of NO_3-N in MBBR K1 increased at a lower rate by 68%, while in the MBBR 3D it increased slightly more than the control MBBR, by 89.5%. It can therefore be concluded that the nitrification process in control MBBR is more efficient than in MBBR K1 and slightly more efficient than in the MBBR 3D. Given that the maximum permissible limits of drinking water pollution for nitrate nitrogen is 45 mg/L, it can also be concluded that, in both MBBR units, the NO_3-N values were within the limits even for drinking water [36], as shown in **Figure 4.**

As shown in **Figure 5,** there was an efficient decrease in NH_4-N concentration in all three MBBR units, leading to an average effluent concentration of about 1.5 mg/L for control MBBR and MBBR K1, while the concentration decreased even more for MBBR 3D, in which it was equal to 0.4 mg/L. The NH_4-N removal rate in control MBBR reached 89.3%, it was slightly lower in MBBR K1 with a value of 88.7%, while in MBBR 3D it reached 98%. Due to the fact that the 3D-printed biocarriers could not move enough inside the unit, more suspended biofilm was developed, something that, combined with the attached biofilm, provided additional nitrification capacity and significantly reduced the amount of ammonia in the effluent [37]. The inside surface of biocarriers is the best place

 doi:10.20944/preprints202306.0207.v1

for developing nitrifying bacteria and in the case of 3D-printed biocarriers, the size of the inside surface was large thanks to the appropriate design of the biocarriers. This explains their increased efficiency in the nitrification process [38].

Finally, the value of Total N removal in control MBBR was 32.5%, in MBBR K1 it was higher (37%) and in MBBR 3D it was even higher (reaching 45%) (**Figure 6**). More specifically, in MBBR K1, the value of Total N in the influent was 37 mg/L and it was reduced to 25 mg/L in the effluent. In MBBR K1, it was reduced a little more; from 37 mg/L in the influent to 23 mg/L in the effluent and finally, in MBBR 3D it started from 34 mg/L and was reduced to 18 mg/L. Consequently, it can be stated that in MBBR K1 and even more in MBBR 3D, the denitrification was more efficient than in control MBBR. This is due to the anoxic conditions created in the formed biofilm on the surfaces of the biocarriers, given that denitrification occurs in the absence of oxygen. The acceptable limit values of Total N for wastewater discharge in water bodies are either a total N value of 10-15 mg/L or a minimum Total N removal rate during wastewater treatment of 70-80% [36]. Based on this, it is concluded that in the first two MBBR cases, the Total N removal rate was reduced, something that made the further treatment of wastewater necessary, while in the third case, a small improvement of the treatment method could potentially provide a sufficient Total N removal.

The value of SMP protein concentration (**Figure 7**) in control MBBR during the aerobic phase was 13 mg/L while during the anoxic phase it was slightly higher. The value of SMP carbohydrates concentration (**Figure 8**) during aeration was 4.2 mg/L, and, similar to the case of the SMP proteins, it was slightly higher during the anoxic phase. However, in the MBBR K1 experiment the average value of SMP proteins concentration was 21 mg/L during the aerobic phase while it did not change a lot during the anoxic phase. The value of SMP carbohydrates concentration during aeration was 3.3 mg/L and during the anoxic phase it was slightly higher. In the MBBR 3D experiment, the value of SMP proteins concentration during aeration was 17 mg/L while during the anoxic phase the value was slightly lower. The value of SMP carbohydrates concentration during aeration was 15 mg/L, while during the anoxic phase it was slightly higher. These results show that the SMP protein concentration increased in MBBR K1 and MBBR 3D by 8 units in the former and 4 units in the latter, as compared to the control MBBR. On the contrary, the SMP carbohydrates concentration remained approximately on the same levels for the first two experiments, but it increased in the activated sludge by 12 units when 3D-printed biocarriers were added.

As opposed to SMPs, the EPS in the activated sludge were reduced in the MBBR K1 compared to the control MBBR. For the aeration stage, the specific values were as follows: in the control MBBR experiment, the value of EPS proteins was 35 mg/g TSS and the value of EPS carbohydrates 18 mg/g TSS, in the MBBR K1 experiment the value of EPS proteins was 20 mg/g TSS and the value of EPS carbohydrates 11 mg/g TSS and, finally in the MBBR 3D experiment the value of EPS proteins was 15 mg/g TSS and the value of EPS carbohydrates was 6.1 mg/g TSS (**Figures 9** and **10** respectively).

Based on the increase of soluble SMPs produced and the decrease of bound EPS in the MBBR K1 and MBBR 3D units, it can be concluded that the growth of nitrifying bacteria and heterotrophs inside the units increased biomass production and soluble SMP generation instead of bound EPS. The generated SMPs favored the adhesion of biomass on the surface of biocarriers [19,20], as shown in **Tables 2** and **3.**

As observed in the standard image of mixed liquor taken from an optical microscope (**Figure 11**), there are filamentous microorganisms protruding from the outer surfaces of the sludge flocculates, with the FI values ranging from 1-2 throughout the operation of the units for all three MBBRs [30].

In relation to the size of the aggregates, it is observed that in K1 biocarriers (**Figure 12 (a)**) there is a very mild tendency for it to increase in the activated sludge, since the aggregates are light and during agitation they break up the developing sludge flocculates. However, this is not the case for 3D-printed biocarriers (**Figure 12 (b)**) in which a larger tendency in the increase of sludge flocculates is observed because they are heavier than K1 and their agitation is much more mild. As a result, sludge flocculates are properly developed in the activated sludge and biofilm is also produced on the surface of the biocarriers, combining attached and suspended biofilm growth.

 doi:10.20944/preprints202306.0207.v1

As shown in **Figure 13**, biofilm is clearly produced not only inside the biocarriers of MBBR K1, but also on the trabecular surfaces of the biocarriers' walls. On the 14th day of the unit operation, it was observed that biofilm was created inside three out of the four quadrants of the biocarrier as well as on its trabecular surfaces. On the 29th day of the unit operation, biofilm was created in all four quadrants of the biocarrier.

The dry mass of the biofilm that was developed in the K1 biocarriers ranged from 3.1-4.5 mg (**Table 2**). These fluctuations in the values are attributed to the large size of the holes in K1 biocarriers, due to which it is not possible to sufficiently maintain the biofilm created. The generated biofilm is quite fluid and as a result it easily detaches due to the aeration and the agitation that take place in the unit. This periodic reduction of biofilm in the biocarriers is the reason for the reduced performance of biocarriers in wastewater treatment using an MBBR K1 unit. Consequently, it could be suggested that biocarriers with smaller but more holes could potentially resolve the issue of biofilm detachment during aerobic wastewater treatment.

In the case of 3D-printed biocarriers with 13X and bentonite, the above issue was resolved, as the biocarriers were produced with holes smaller in size but more in quantity. As shown in **Figure 14** and mostly in **Table 3**, 3D-printed biocarriers managed to hold much more biofilm mass, ranging from 641-867 mg, which means that the biofilm mass was 2 orders of magnitude larger compared to K1 biocarriers. A small fluctuation in the values is also observed in this case during the operation of the units, which is due to the aeration. Nevertheless, this can be considered negligible, as most of the biofilm is retained inside the holes protected. The very high biofilm growth and retention in the case of 3D biocarriers is the reason why the nitrification and denitrification performance during wastewater treatment was significantly improved while EPS proteins and carbohydrates in the mixed liquor activated sludge were reduced.

According to **Figure 15**, the microbial community analysis showed an enhanced presence of the *Clostridia* class in the 3D-printed biocarriers, which have sulfate-reducing capabilities [39] and are known glucose fermenters, generating products critically involved in methane production [40]. Their greater prevalence together with *Bacilli* compared to K1 ring may indicate that 3D-printed biocarriers are likely to favor the formation of thicker biofilm, composed of anaerobic bacterial groups that are linked to methane production pathways. Moreover, *Exiguobacterium*, belonging to *Bacillales Incertae Sedis family XII*, which were found in higher abundance in 3D-printed carriers than in K1 or sludge, have been reported to form biofilm on the surface of biocarriers [41]. Another genus found more enriched in 3D-printed biocarriers compared to K1 was *Trichococcus* (*Carnobacteriaceae*), which is involved in the degradation of various substrates, like polysaccharides, alcohols, and sugars [42] and participates in denitrification [43]. Additionally, *Phenylobacterium* (*Caulobacteraceae*) is a genus more commonly observed along with biofilm succession, due to limited motility, which potentially hampers its ability to colonize surfaces early on [44]. Of note, this genus was more evident in the biofilm of 3D-printed biocarriers in comparison with the one of K1 ring, corroborating the possibility of a faster biofilm formation on the surface of 3D-printed carriers. *Acinetobacter* (*Moraxellaceae*), on the other hand, were substantially more abundant in K1 than in both the 3D-printed carriers and the sludge. This group is implicated in denitrification, nitrification, and phosphorus removal, however its function in fermentation can be readily substituted by other fermenters under anaerobic conditions [45]. *Rhodobacteraceae*, mainly composed of *Gemmobacter* and *Paracoccus*, was also found higher in numbers in the biofilm of K1 ring, and members of this group are typically among the first organisms to colonize and contribute to biofilm formation [46], suggesting that the biofilm development on K1 carrier might be in a more primary stage at the time of sampling.

5. Conclusions

The findings of this research suggest that the effluent quality in relation to COD removal for all three MBBR units is excellent since the removal rate percentage reaches 84-92%. During the outflow phase in the unit, the value of NO_3-N was increased by 89% in control MBBR, by 68% in MBBR K1 and by 89.5% in MBBR 3D. The NH_4-N removal rate reached 89.3% in control MBBR, 88.7% in MBBR K1, while it reached 98% in MBBR 3D. Finally, the value of Total N removal was 32.5% in control

 doi:10.20944/preprints202306.0207.v1

MBBR, 37% in MBBR K1 and 45% in MBBR 3D. For all three parameters, it is clear that the addition of 3D-printed biocarriers is the most profitable option, as it allows the nitrification and denitrification processes to be carried out more efficiently due to the growth of a large amount of biofilm, which is kept protected in the biocarriers' holes for the whole duration of the unit operation. The inside of the biocarriers is the most suitable area for nitrifying bacteria growth. The nitrifying bacteria help improve nitrification and at the same time create anoxic conditions in the inside of biofilm which improves denitrification.

More specifically, the dry mass of the biofilm that was developed in the K1 biocarriers ranged from 3.1-4.5 mg, while in 3D-printed biocarriers it was increased by two orders of magnitude to 641-867 mg. What is more, in the K1 biocarriers, the mass of the biofilm fluctuated in relation to time, due to the fact that they could not keep the biofilm inside the holes, something that was not observed in the 3D-printed biocarriers.

Furthermore, it can be concluded that the cumulative values of soluble SMP increased from 17 mg/L in control MBBR, to 24 mg/L in MBBR K1 and to 32 mg/L in MBBR 3D. Therefore, it is concluded that the growth of nitrifying bacteria and heterotrophs inside the units, increased biomass production in the form of soluble SMP, which in turn favored the adhesion of biomass on the surface of biocarriers.

Author Contributions: Funding acquisition, Themistoklis Sfetsas ; Investigation, Dimitra Banti; Methodology, Dimitra Banti, Afroditi Chioti, Anastasios Mitsopoulos and Michail Tsangas; Software, Dimitra Banti; Supervision, Dimitra Banti, Petros Samaras and Themistoklis Sfetsas ; Validation, Dimitra Banti, Petros Samaras, Afroditi Chioti, Anastasios Mitsopoulos and Antonis Zorpas; Writing – original draft, Dimitra Banti; Writing – review & editing, Dimitra Banti.

Funding: This research was co-funded by the European Regional Development Fund of the European Union and Greek national funds through the Operational Program Competitiveness, Entrepreneurship and Innovation, under the call RESEARCH—CREATE—INNOVATE (project code: T2EDK-00362).

Data Availability Statement: Data presented in this study are available upon request from the corresponding author.

Conflicts of Interest: The authors declare that they have no known competing financial interest or personal relationship that could have appeared to influence the work reported in this paper.

References

1. Boltz, J.; Boltz, J.P.; Smets, B.F.; Rittmann, B.E.; Loosdrecht, M.C.M. Van; Morgenroth, E.; Daigger, G.T. From biofilm ecology to reactors : A focused review From bio fi lm ecology to reactors : a focused review. **2017**.
2. Kawan, J.A.; Abu Hasan, H.; Suja, F.; Jaafar, O.; Abd-Rahman, R. A review on sewage treatment and polishing using moving bed bioreactor (Mbbr). *Journal of Engineering Science and Technology* **2016**, *11*, 1098–1120.
3. Avellán, T.; Hahn, A.; Kirschke, S.; Müller, A.; Benavides, L.; Caucci, S. Co-Generating Knowledge in Nexus Research for Sustainable Wastewater Treatment. *Resources* **2022**, *11*.
4. Banti, D.C.; Tsangas, M.; Samaras, P.; Zorpas, A. LCA of a membrane bioreactor compared to activated sludge system for municipal wastewater treatment. *Membranes* **2020**, *10*, 1–15.
5. Lemonidis, I.; Banti, D.C.; Tzenos, C.A.; Kalamaras, S.D.; Kotsopoulos, T.A.; Samaras, P. Energy Valorization of Fine Screenings from a Municipal Wastewater Treatment Plant. *Energies* **2022**, *15*.
6. Conserva, S.; Tatti, F.; Torretta, V.; Ferronato, N.; Viotti, P. An integrated approach to the biological reactor-sedimentation tank system. *Resources* **2019**, *8*.
7. Dong, Y.; Fan, S.Q.; Shen, Y.; Yang, J.X.; Yan, P.; Chen, Y.P.; Li, J.; Guo, J.S.; Duan, X.M.; Fang, F.; et al. A Novel Bio-carrier Fabricated Using 3D Printing Technique for Wastewater Treatment. *Scientific Reports* **2015**, *5*.
8. Tang, B.; Song, H.; Bin, L.; Huang, S.; Zhang, W.; Fu, F.; Zhao, Y.; Chen, Q. Bioresource Technology

Determination of the profile of DO and its mass transferring coefficient in a biofilm reactor packed with semi-suspended bio-carriers. *Bioresource Technology* **2017**, *241*, 54–62.

9. Gerard, M.H. *Troubleshooting the sequencing batch reactor*; John Wiley & Sons, Inc., Publication, 2011; ISBN 9781118058220.
10. Poltak, R.F. Sequencing Batch Reactor Design and Operational Considerations Manual. *New England Interstate Water Pollution Control Commission: Massachusetts, USA* **2005**, 27.
11. Barwal, A.; Chaudhary, R. To study the performance of biocarriers in moving bed biofilm reactor (MBBR) technology and kinetics of biofilm for retrofitting the existing aerobic treatment systems : a review. **2014**, 285–299.
12. Felföldi, T.; Jurecska, L.; Vajna, B.; Barkács, K.; Makk, J.; Cebe, G.; Szabó, A.; Záray, G.; Márialigeti, K. Texture and type of polymer fiber carrier determine bacterial colonization and biofilm properties in wastewater treatment. **2015**, *264*, 824–834.
13. Elliott, O.; Gray, S.; Mcclay, M.; Nassief, B.; Nunnelley, A.; Ekong, J.; Kardel, K.; Khoshkhoo, A.; Proaño, G.; David, M.; et al. Design and Manufacturing of High Surface Area 3D-Printed Media for Moving Bed Bioreactors for Wastewater Treatment. **2017**, 144–156.
14. Proano-Pena, G.; Carrano, A.L.; Blersch, D.M. Analysis of very-high surface area 3D-printed media in a moving bed biofilm reactor for wastewater treatment. *PLoS ONE* **2020**, *15*, 1–17.
15. Chioti, A.G.; Tsioni, V.; Patsatzis, S.; Filidou, E.; Banti, D.; Samaras, P.; Economou, E.A.; Kostopoulou, E.; Sfetsas, T. Characterization of Biofilm Microbiome Formation Developed on Novel 3D-Printed Zeolite Biocarriers during Aerobic and Anaerobic Digestion Processes. **2022**.
16. Al-amshawee, S.K.A.; Bin, Y.; Yunus, M. Experimental investigation of bio fi lm carriers of varying shapes , sizes , and materials for wastewater treatment in fi xed bed bio fi lm reactor : a qualitative study of biocarrier performance. **2022**.
17. Gkotsis, P.; Banti, D.; Pritsa, A.; Mitrakas, M.; Samaras, P.; Peleka, E.; Zouboulis, A. Effect of operating conditions on membrane fouling in pilot-scale mbrs; filaments growth, diminishing dissolved oxygen and recirculation rate of the activated sludge. *Membranes* **2021**, *11*, 1–16.
18. Lin, H.; Zhang, M.; Wang, F.; Meng, F.; Liao, B.Q.; Hong, H.; Chen, J.; Gao, W. A critical review of extracellular polymeric substances (EPSs) in membrane bioreactors: Characteristics, roles in membrane fouling and control strategies. *Journal of Membrane Science* **2014**, *460*, 110–125.
19. Bassin, J.P.; Kleerebezem, R.; Rosado, A.S.; Van Loosdrecht, M.C.M.; Dezotti, M. Effect of different operational conditions on biofilm development, nitrification, and nitrifying microbial population in moving-bed biofilm reactors. *Environmental Science and Technology* **2012**, *46*, 1546–1555.
20. Gupta, B.; Kumar, A.; Sarathi, P.; Lal, S. Journal of Environmental Chemical Engineering Recent advances in application of moving bed biofilm reactor for wastewater treatment : Insights into critical operational parameters , modifications , field-scale performance , and sustainable aspects. *Journal of Environmental Chemical Engineering* **2022**, *10*, 107742.
21. Banti, D.C.; Karayannakidis, P.D.; Samaras, P.; Mitrakas, M.G. An innovative bioreactor set-up that reduces membrane fouling by adjusting the filamentous bacterial population. *Journal of Membrane Science* **2017**.
22. Banti, D.; Mitrakas, M.; Fytianos, G.; Tsali, A.; Samaras, P. Combined effect of colloids and SMP on membrane fouling in MBRs. *Membranes* **2020**, *10*, 1–15.
23. Mandakhalikar, K.D.; Rahmat, J.N.; Chiong, E.; Neoh, K.G.; Shen, L.; Tambyah, P.A. Extraction and quantification of biofilm bacteria: Method optimized for urinary catheters. *Scientific Reports* **2018**, *8*, 1–9.
24. Mohamed, A.; Rajaa, A.M.; Khalid, Z.; Fouad, M.; Naima, R. Comparison of three methods for the detection of biofilm formation by clinical isolates of Staphylococcus aureus isolated in Casablanca. *International Journal of Science and Research* **2013**, *5*, 2319–7064.
25. APHA (American Public Health Association) *Standard Methods for the Examination of Water and Wastewater*; Washington, DC, 1998;
26. Hwang, B.K.; Kim, J.H.; Ahn, C.H.; Lee, C.H.; Song, J.Y.; Ra, Y.H. Effect of disintegrated sludge recycling on membrane permeability in a membrane bioreactor combined with a turbulent jet flow ozone contactor. *Water Research* **2010**, *44*, 1833–1840.
27. Banti, D.C.; Samaras, P.; Tsioptsias, C.; Zouboulis, A.; Mitrakas, M. Mechanism of SMP aggregation within the pores of hydrophilic and hydrophobic MBR membranes and aggregates detachment. *Separation and Purification Technology* **2018**.
28. Hartree, E.F. Determination of protein: A modification of the Lowry method that gives a lineart photometric response. *Analytical Biochemistry* **1972**, *48*.
29. Dubois, M.; Gilles, K.A.; Hamilton, J.K.; Rebers, P.A.; Smith, F. Colorimetric Method for Determination of Sugars and Related Substances. **1956**, 350–356.

30. Eikelboom, D.H. *Process control of activated sludge plants by microscopic investigation*; IWA Publishing: Zutphen, 2000;
31. Banti, D.C.; Mitrakas, M.; Samaras, P. Membrane fouling controlled by adjustment of biological treatment parameters in step-aerating MBR. *Membranes* **2021**, *11*, 1–15.
32. Bolyen, E.; Rideout, J.R.; Dillon, M.R.; Bokulich, N.A.; Abnet, C.C.; Al-Ghalith, G.A.; Alexander, H.; Alm, E.J.; Arumugam, M.; Asnicar, F.; et al. Reproducible, interactive, scalable and extensible microbiome data science using QIIME 2. *Nature Biotechnology* **2019**, *37*, 852–857.
33. Benjamin, C.; McMurdie, P.; Rosen, M.; Han, A.; Johnson, A.; Holmes, S. DADA2:High resolution sample inference from Illumina amplicon data. *Encyclopedia of Medical Immunology* **2020**, *13*, 1–7.
34. Quast, C.; Pruesse, E.; Yilmaz, P.; Gerken, J.; Schweer, T.; Yarza, P.; Peplies, J.; Glöckner, F.O. The SILVA ribosomal RNA gene database project: Improved data processing and web-based tools. *Nucleic Acids Research* **2013**, *41*, 590–596.
35. Banti, D.C.; Tsali, A.; Mitrakas, M.; Samaras, P. The Dissolved Oxygen Effect on the Controlled Growth of Filamentous Microorganisms in Membrane Bioreactors. **2020**, *i*, 39.
36. Guidelines, G.E.H.S. Environmental , Health , and Safety General Guidelines. **2007**.
37. Waqas, S.; Harun, N.Y.; Sambudi, N.S.; Abioye, K.J.; Hamad, M. A review on integrated fixed-film activated sludge for the treat- ment of wastewater. **2023**, 1–22.
38. Waqas, S.; Bilad, M.R.; Man, Z.B. Performance and energy consumption evaluation of rotating biological contactor for domestic wastewater treatment. *Indonesian Journal of Science and Technology* **2021**, *6*, 101–112.
39. Biswas, K.; Turner, S.J. Microbial community composition and dynamics of moving bed biofilm reactor systems treating municipal sewage. *Applied and Environmental Microbiology* **2012**, *78*, 855–864.
40. Chioti, A.G.; Tsioni, V.; Patsatzis, S.; Filidou, E.; Banti, D.; Samaras, P.; Economou, E.A.; Kostopoulou, E.; Sfetsas, T. Characterization of Biofilm Microbiome Formation Developed on Novel 3D-Printed Zeolite Biocarriers during Aerobic and Anaerobic Digestion Processes. *Fermentation* **2022**, *8*.
41. Sakdapetsiri, C.; Kaokhum, N.; Pinyakong, O. Biodegradation of crude oil by immobilized Exiguobacterium sp. AO-11 and shelf life evaluation. *Scientific Reports* **2021**, *11*, 1–13.
42. Doloman, A.; Boeren, S.; Miller, C.D.; Sousa, D.Z. Stimulating Effect of Trichococcus flocculiformis on a Coculture of Syntrophomonas wolfei and Methanospirillum hungatei. *Applied and Environmental Microbiology* **2022**, *88*, 1–14.
43. Rodriguez-Sanchez, A.; Muñoz-Palazon, B.; Hurtado-Martinez, M.; Mikola, A.; Gonzalez-Lopez, J.; Vahala, R.; Gonzalez-Martinez, A. Analysis of microbial communities involved in organic matter and nitrogen removal in a full-scale moving bed biofilm reactor located near the Polar Arctic Circle. *International Biodeterioration and Biodegradation* **2020**, *146*, 104830.
44. Niederdorfer, R.; Besemer, K.; Battin, T.J.; Peter, H. Ecological strategies and metabolic trade-offs of complex environmental biofilms. *npj Biofilms and Microbiomes* **2017**, *3*.
45. Cheng, H.; Cheng, D.; Mao, J.; Lu, T.; Hong, P.Y. Identification and characterization of core sludge and biofilm microbiota in anaerobic membrane bioreactors. *Environment International* **2019**, *133*.
46. Cinà, P.; Bacci, G.; Arancio, W.; Gallo, G.; Fani, R.; Puglia, A.M.; Di Trapani, D.; Mannina, G. Assessment and characterization of the bacterial community structure in advanced activated sludge systems. *Bioresource Technology* **2019**, *282*, 254–261.